Thermodynamical analysis of a quantum heat engine based on harmonic oscillators

Andrea Insinga[*] and Bjarne Andresen[†]
Niels Bohr Institute, University of Copenhagen, Universitetsparken 5, DK-2100 Copenhagen Ø, Denmark

Peter Salamon[‡]
Department of Mathematics and Statistics, San Diego State University, San Diego, California 92182-7720, USA
(Received 11 April 2016; published 15 July 2016)

Many models of heat engines have been studied with the tools of finite-time thermodynamics and an ensemble of independent quantum systems as the working fluid. Because of their convenient analytical properties, harmonic oscillators are the most frequently used example of a quantum system. We analyze different thermodynamical aspects with the final aim of the optimization of the performance of the engine in terms of the mechanical power provided during a finite-time Otto cycle. The heat exchange mechanism between the working fluid and the thermal reservoirs is provided by the Lindblad formalism. We describe an analytical method to find the limit cycle and give conditions for a stable limit cycle to exist. We explore the power production landscape as the duration of the four branches of the cycle are varied for short times, intermediate times, and special frictionless times. For short times we find a periodic structure with atolls of purely dissipative operation surrounding islands of divergent behavior where, rather than tending to a limit cycle, the working fluid accumulates more and more energy. For frictionless times the periodic structure is gone and we come very close to the global optimal operation. The global optimum is found and interestingly comes with a particular value of the cycle time.

DOI: 10.1103/PhysRevE.94.012119

I. INTRODUCTION

The theory of quantum mechanics was originally developed to describe closed systems, governed by a unitary equation of motion. More recently, the topic of open quantum systems has been the object of many studies, and different approaches have been developed for the evolution equation governing such systems [1]. One of these approaches is the Lindblad formalism [2]: The quantum system interacts with two larger systems, called *heat reservoirs*, which are not perturbed significantly by the interaction and therefore remain for the whole duration of the evolution in the thermal equilibrium state, determined for each reservoir by a single parameter, β, called the *inverse temperature*. The effect of this interaction on the smaller system is taken into account as an additional nonunitary term in the evolution equation governing its dynamics. Because of this term the energy is time dependent and its variation is interpreted as heat exchange.

Within the topic of dissipative quantum systems, it is possible to find many works about the analysis of models for quantum heat engines [3–6] and quantum refrigerators [7,8]. The description of a thermodynamic cycle requires the combination of the dissipative dynamics, caused by the interaction with a thermal reservoir, and the unitary dynamics with an explicitly time-dependent Hamiltonian, that is, the model for the mechanical work exchange mechanism.

The interest in this topic is partly due to the relation with the experimental field of atomic and molecular cooling. In particular, with the use of the *quantum refrigerator* model it has been possible to investigate the characteristics and limits of cooling mechanisms when systems approach absolute zero temperature [7]. Here it is of course necessary to use a quantum description. The analysis of models for a *quantum heat engine* is also interesting because of its connection to *Finite-time thermodynamics*. This theory deals with a thermodynamic system which is subject to processes that take place in a finite amount of time and for this reason must deviate from equilibrium. Different papers [9–11] within this field analyze the optimal performance of a heat engine, i.e., the maximum possible mechanical power that a heat engine is able to supply when it is driven by finite-time transformations. The quantum models for heat engines have been studied recently from the same perspective with very interesting results.

The working medium of these thermodynamic devices is modeled by a statistical ensemble of noninteracting quantum systems. They can be spin systems interacting with external magnetic fields and characterized by a finite number of degrees of freedom [4,8,12] or quantum particles confined in a position dependent potential. Because of its convenient properties the harmonic potential is the example of a potential most frequently encountered in the literature [5–7].

In this work we focus on a working medium composed of an ensemble of quantum harmonic oscillators, and we analyze the time evolution in the Heisenberg picture. We consider a set of Hermitian operators forming a Lie algebra which is closed under the equations of motions, for which the analytical solution can be calculated. In Sec. II G we introduce an analogy between homogeneous coordinate systems and the set of operators in the algebra and show how this analogy leads to a closed-form expression for the limit-cycle solution and allows us to classify the stability of this solution.

We adopt an optimization perspective and, following previous works in finite-time quantum thermodynamics [4,5], we select as objective the total mechanical power averaged over one cycle of operation. We optimize the total power with respect to the times allocated for the four different processes of the thermodynamic cycle. As we explain in Sec. IV B, there

[*]Email addresses: andreainsinga@gmail.com
[†]Email addresses: andresen@nbi.ku.dk
[‡]Email addresses: salamon@math.sdsu.edu

exist special choices of the time allocated for the adiabatic processes which lead to frictionless cycles. These special times are linked with the occurrence of a periodic power landscape and are relevant to our optimization problem.

II. METHODS

A. The system

The system is an ensemble of independent harmonic oscillators, governed by the Hamiltonian represented by the operator $\hat{H}$:

$$\hat{H}(t) = \frac{1}{2m}\hat{P}^2 + \frac{1}{2}m[\omega(t)]^2\,\hat{Q}^2, \tag{1}$$

where $\hat{Q}$ and $\hat{P}$ are the position and momentum operators, m is the mass, and ω the frequency of the oscillators. The frequency ω is the only explicitly time-dependent part of the Hamiltonian.

The Lagrangian of the system is represented by the operator $\hat{L}$:

$$\hat{L}(t) = \frac{1}{2m}\hat{P}^2 - \frac{1}{2}m[\omega(t)]^2\,\hat{Q}^2. \tag{2}$$

Another operator which will be relevant is the correlation operator $\hat{C}$:

$$\hat{C}(t) = \tfrac{1}{2}\omega(t)(\hat{Q}\hat{P} + \hat{P}\hat{Q}). \tag{3}$$

Moreover, the annihilation operator $\hat{a}$ and the creation operator $\hat{a}^\dagger$ will be considered:

$$\hat{a} = \frac{1}{\sqrt{2}}\left[\left(\frac{\sqrt{m\omega}}{\sqrt{\hbar}}\right)\hat{Q} + i\left(\frac{1}{\sqrt{m\omega\hbar}}\right)\hat{P}\right], \tag{4}$$

$$\hat{a}^\dagger = \frac{1}{\sqrt{2}}\left[\left(\frac{\sqrt{m\omega}}{\sqrt{\hbar}}\right)\hat{Q} - i\left(\frac{1}{\sqrt{m\omega\hbar}}\right)\hat{P}\right]. \tag{5}$$

The state of the ensemble of systems is represented by the density operator $\hat{\rho}$, which is time independent in the Heisenberg picture.

The expectation values of an operator $\hat{X}$ at the time t is given by

$$\langle\hat{X}\rangle(t) = \mathrm{Tr}[\hat{\rho}\hat{X}(t)]. \tag{6}$$

The expectation value $\langle\hat{X}\rangle$ will also be simply denoted by X.

B. Time evolution

We will consider the time evolution of the ensemble of oscillators using the Heisenberg picture. As it will be explained in more detail in Sec. II C, when the system obeys canonical invariance it is possible to use the Heisenberg picture to calculate the evolution of the expectation values of a finite set of operators forming a Lie algebra without the necessity to specify anything else about the state of the system. This allows us to calculate the mechanical power production, which, as will be explained in Sec. IV A, is the objective of our optimization problem.

The equation of motion for an operator $\hat{X}$ in the Heisenberg picture can be written as

$$\frac{d}{dt}\hat{X}(t) = \mathcal{L}_H^*[\hat{X}(t)] + \mathcal{L}_D^*[\hat{X}(t)] + \frac{\partial}{\partial t}\hat{X}(t), \tag{7}$$

where $\partial\hat{X}/\partial t$ is the explicit time dependence of the operator, $\mathcal{L}_H^*$ is the superoperator representing the unitary part of the evolution, and $\mathcal{L}_D^*$ is the superoperator representing the nonunitary part of the evolution which arises from the dissipative interaction of the system with the heat reservoirs. The symbol * represents the adjoint of the corresponding superoperators which govern the evolution of $\hat{\rho}$ in the Schrödinger picture.

The unitary superoperator is given by

$$\mathcal{L}_H^*(\hat{X}_j) = \frac{i}{\hbar}[\hat{H}(t), \hat{X}(t)]. \tag{8}$$

Since during the isochore phases ω is constant, we are interested in the Lindblad superoperator for the harmonic oscillator with a time-independent Hamiltonian which is given by

$$\begin{aligned}\mathcal{L}_D^*(\hat{X}) = {} & k_\downarrow\left(\hat{a}^\dagger\hat{X}\hat{a} - \tfrac{1}{2}\left\{\hat{a}^\dagger\hat{a}, \hat{X}\right\}\right) \\ & + k_\uparrow\left(\hat{a}\hat{X}\hat{a}^\dagger - \tfrac{1}{2}\left\{\hat{a}\hat{a}^\dagger, \hat{X}\right\}\right).\end{aligned} \tag{9}$$

The two coefficients $k_\uparrow$ and $k_\downarrow$ are known as transition rates. In order for the detailed balance condition to be obeyed, the ratio between the transition rates must satisfy $k_\uparrow/k_\downarrow = \exp(-\beta\hbar\omega)$, where $\beta = 1/k_B T$ is the inverse temperature. This requirement still allows us to arbitrarily define the net transition rate $\Gamma = k_\downarrow - k_\uparrow$, also called the heat conductance.

C. Canonical invariance

For the harmonic system a finite set of Hermitian operators $\hat{X}_k$ can be defined so their general evolution can be written in the closed form,

$$\frac{d}{dt}\hat{X}_j(t) = \sum_{k=1}^{K} a_{jk}(t)\,\hat{X}_k(t) \quad \text{with} \quad a_{jk} \in \mathbb{R}, \tag{10}$$

which can be written in matrix notation as

$$\frac{d}{dt}\underline{\hat{X}}(t) = \boldsymbol{A}(t)\,\underline{\hat{X}}(t). \tag{11}$$

This property follows from the fact that the operators form a closed Lie algebra and that the system exhibits canonical invariance. In the Schrödinger picture the property called canonical invariance is when an initially canonical form for the density matrix, $\hat{\rho} = (1/Z)\exp(\sum_k \beta_k\hat{X}_k)$, retains this form at all instants of time. The density operator $\hat{\rho}$ is completely parametrized by the time dependence of the coefficients $\beta_k(t)$.

The first requirement for this condition to be satisfied is that the operators form a closed Lie algebra:

$$[i\,\hat{X}_h, i\,\hat{X}_j] = i\sum_{k=1}^{K}\Gamma_{hjk}\hat{X}_k \quad \text{with} \quad \Gamma_{hjk} \in \mathbb{R} \quad \forall\, h,j,k. \tag{12}$$

For adiabatic evolution the second condition is that the algebra is closed with respect to $\mathcal{L}_H^*$, which is true if the Hamiltonian operator can be expressed as a linear combination of the

operators in the set:

$$\hat{H} = \sum_{k=1}^{K} c_k \hat{X}_k \quad \text{with} \quad c_k \in \mathbb{R} \quad \forall\, k. \tag{13}$$

For isochoric evolution the algebra must be closed with respect to $\mathcal{L}_D^*$, and it can be shown [5] that canonical invariance is satisfied with the Lindblad superoperator defined in Eq. (9).

The basis of canonically invariant Hermitian operators is not uniquely defined; for example, one possible choice is $\{\hat{X}_j\} = \{\hat{Q}^2, \hat{P}^2, \hat{Q}\hat{P} + \hat{P}\hat{Q}, \hat{1}\}$. In this work, we adopt another choice which is commonly found in the literature:

$$\{\hat{X}_j\} = \{\hat{H}, \hat{L}, \hat{C}, \hat{1}\}. \tag{14}$$

Since the evolution equation is linear, the general solution can be expressed as

$$\underline{\hat{X}}(t) = \boldsymbol{U}(t)\, \underline{\hat{X}}(0), \tag{15}$$

where the matrix $\boldsymbol{U}$ is the evolution matrix and satisfies the linear differential equation

$$\frac{d}{dt}\boldsymbol{U}(t) = \boldsymbol{A}(t)\boldsymbol{U}(t) \tag{16}$$

with the initial condition $\boldsymbol{U}(0) = \mathbf{1}$.

D. The Otto cycle

The ensemble undergoes a thermodynamic cycle composed of four branches. To avoid the mathematical difficulties of considering a time-dependent Hamiltonian at the same time as the dissipative evolution, the Otto cycle is chosen for which heat transfer and mechanical work transfer never occur simultaneously. One complete thermodynamic Otto cycle is composed of the following four processes in order:

(1) *Hot isochore*: The system, whose frequency is equal to ω_H, is coupled to the hot heat reservoir whose inverse temperature is denoted by β_H. The heat conductance is equal to Γ_H.

(2) *Expansion adiabat*: The frequency of the system changes from ω_H to ω_C with no connection to any of the heat reservoirs.

(3) *Cold isochore*: The system, whose frequency is equal to ω_C, is coupled to the cold heat reservoir whose inverse temperature is denoted by β_C. The heat conductance is equal to Γ_C.

(4) *Compression adiabat*: The frequency of the system changes from ω_C to ω_H with no connection to any of the heat reservoirs.

The durations of the four processes are denoted respectively by τ_H, τ_{HC}, τ_C, and τ_{CH}, making the duration of a complete cycle $\tau = \tau_H + \tau_{HC} + \tau_C + \tau_{CH}$. The following relations need to be satisfied by the choice of parameters: $\beta_C > \beta_H$ and $\omega_C < \omega_H$.

Similarly, the evolution matrices for the four branches are denoted respectively by $\boldsymbol{U}_H$, $\boldsymbol{U}_{HC}$, $\boldsymbol{U}_C$, and $\boldsymbol{U}_{CH}$. The evolution matrix $\boldsymbol{U}(\tau)$ for one cycle can then be factorized as $\boldsymbol{U}(\tau) = \boldsymbol{U}_{CH}\boldsymbol{U}_C\boldsymbol{U}_{HC}\boldsymbol{U}_H$.

E. Adiabat dynamics

During the *adiabatic processes* the parameter ω is time dependent and therefore the energy $\langle\hat{H}\rangle$ of the system may vary. This energy variation is interpreted as the work exchange of the system. However, part of this work is associated with a change in the probability distribution among the energy levels and to the concept of *quantum friction* [4,13].

There are many possible choices for the time dependence of the frequency $\omega(t)$, the three following examples being the simplest: (i) linear evolution for which $\dot{\omega}$ is constant; (ii) exponential evolution for which the relative rate of change (also called nonadiabatic parameter), $\lambda = \dot{\omega}/\omega$, is constant; and (iii) Shortcut To Adiabaticity (STA) evolution for which the dimensionless adiabatic parameter, $\mu = \dot{\omega}/\omega^2$, is constant. This choice may be critical since a particular time dependence of ω could lead to an equation that can be solved analytically. As explained in Ref. [7], this useful property is satisfied for choice (iii) for which μ is constant. Even though it would not make a substantial difference to choose one or the other when a numerical method is employed for the integration of the evolution equations, we used the time dependence with constant μ for our simulations. In this way, the properties of the harmonic solution can be employed to predict the qualitative behavior of the power landscape and provide a useful starting point for the optimization problem; μ is zero during isochore phases.

The evolution of $\underline{X}$ can be calculated from Eq. (7) without the dissipative term $\mathcal{L}_D^*$ by considering the appropriate ω time dependence and calculating the various commutators between the operators. This leads to the following equation:

$$\frac{d}{dt}\begin{pmatrix} H \\ L \\ C \\ 1 \end{pmatrix} = \omega(t)\begin{pmatrix} \mu & -\mu & 0 & 0 \\ -\mu & \mu & -2 & 0 \\ 0 & 2 & \mu & 0 \\ 0 & 0 & 0 & 0 \end{pmatrix}\begin{pmatrix} H \\ L \\ C \\ 1 \end{pmatrix}. \tag{17}$$

For this choice of evolution the evolution matrix $\boldsymbol{U}^{\text{adiabat}}$ from the initial to the final instant of the branch can be calculated analytically [7].

The energy variation $\mathcal{P}_{\text{tot}} = dH/dt$ during the adiabat branches is interpreted as the mechanical work exchange rate.

F. Isochore dynamics

During the *isochoric processes* the Hamiltonian does not depend explicitly on time. The dissipation mechanism is included as the nonunitary term $\mathcal{L}_D^*$ visible in Eq. (7) and defined in Eq. (9). The evolution for the isochore branch can be expressed in terms of $H_{\text{eq}} = (\hbar\omega/2)\coth(\beta\hbar\omega/2)$, the thermal equilibrium energy corresponding to the inverse temperature β. As will be clear, its value is also the long-time limit of H.

The evolution of $\underline{X}$, which can be derived from Eq. (7) by calculating the various commutators and anticommutators, is expressed by the following equation:

$$\frac{d}{dt}\begin{pmatrix} H \\ L \\ C \\ 1 \end{pmatrix} = \begin{pmatrix} -\Gamma & 0 & 0 & +\Gamma H_{\text{eq}} \\ 0 & -\Gamma & -2\omega & 0 \\ 0 & +2\omega & -\Gamma & 0 \\ 0 & 0 & 0 & 0 \end{pmatrix}\begin{pmatrix} H \\ L \\ C \\ 1 \end{pmatrix}. \tag{18}$$

The evolution matrix $\boldsymbol{U}^{\text{isochore}}$ from the initial to the final instant of this branch can also be calculated analytically [7].

The energy variation $\dot{Q} = dH/dt$ during the isochore phases is interpreted as the heat exchange rate.

G. Limit cycle

The evolution is periodic with period τ. This is expressed by the equation $\boldsymbol{A}(t+\tau) = \boldsymbol{A}(t)$, which is satisfied by the matrix $\boldsymbol{A}$ introduced in Eq. (11), independently of the choice of a basis on the Lie algebra. The evolution matrix $\boldsymbol{U}$ will then satisfy the property $\boldsymbol{U}(t+\tau) = \boldsymbol{U}(t)\boldsymbol{U}(\tau)$.

Since the expectation value of $\hat{1}$ is always 1, it is insightful to consider the analogy with homogeneous coordinate systems. We will denote with the symbol ˜ the 3×1 vectors and 3×3 matrix blocks acting on the first three variables H, L, and C. In this notation, the evolution equation is written as

$$\boldsymbol{A}(t) = \left(\begin{array}{ccc|c} & \tilde{\boldsymbol{A}}(t) & & \underline{\tilde{B}}(t) \\ \hline 0 & 0 & 0 & 0 \end{array}\right), \tag{19}$$

which results in an evolution matrix of the form

$$\boldsymbol{U}(t) = \left(\begin{array}{ccc|c} & \tilde{\boldsymbol{U}}(t) & & \underline{\tilde{C}}(t) \\ \hline 0 & 0 & 0 & 1 \end{array}\right). \tag{20}$$

The 3×3 matrix $\tilde{\boldsymbol{U}}$ is the linear part of the evolution; the vector $\underline{\tilde{C}}$ can be interpreted as a translation in the space of the first three variables.

For a single cycle evolution we have

$$\underline{\tilde{X}}(t+\tau) = \tilde{\boldsymbol{U}}(\tau)\underline{\tilde{X}}(t) + \underline{\tilde{C}}(\tau), \tag{21}$$

which leads to the following solution for a stationary point $\underline{\tilde{X}}^0$ at the time $t = 0$:

$$\underline{\tilde{X}}^0 = \tilde{\boldsymbol{U}}(\tau)\underline{\tilde{X}}^0 + \underline{\tilde{C}}(\tau) = [\tilde{\mathbf{1}} - \tilde{\boldsymbol{U}}(\tau)]^{-1}\,\underline{\tilde{C}}(\tau). \tag{22}$$

Consequently, the only requirement for the existence of a stationary solution is the invertibility of $\tilde{\mathbf{1}} - \tilde{\boldsymbol{U}}(\tau)$.

As is pointed out in Ref. [6], the stationary solution is not necessarily a stable equilibrium solution. For the evolution equations under consideration, a stable equilibrium point $\underline{\tilde{X}}^0$ also satisfies the following requirement for an arbitrary initial state $\underline{\tilde{X}}(0)$:

$$\lim_{n\to+\infty} \underline{\tilde{X}}(n\tau) = \underline{\tilde{X}}^0. \tag{23}$$

The evolution equation for n cycles can be factorized in the following form:

$$\underline{\tilde{X}}(n\tau) = \tilde{\boldsymbol{U}}^n(\tau)\underline{\tilde{X}}(0) + \sum_{k=0}^{n-1} \tilde{\boldsymbol{U}}^k(\tau)\underline{\tilde{C}}(\tau). \tag{24}$$

It is evident that, in order for the equilibrium solution to be independent of the initial state, the following equation must be satisfied:

$$\lim_{n\to+\infty} \tilde{\boldsymbol{U}}^n(\tau) = \tilde{\mathbf{0}}. \tag{25}$$

This is true if and only if the moduli of all the eigenvalues of the matrix $\tilde{\boldsymbol{U}}(\tau)$ are strictly smaller than 1. This also implies that the geometric series generated by $\tilde{\boldsymbol{U}}(\tau)$ is convergent and the limit is given by

$$\lim_{n\to+\infty} \sum_{k=0}^{n-1} \tilde{\boldsymbol{U}}^k(\tau) = [\tilde{\mathbf{1}} - \tilde{\boldsymbol{U}}(\tau)]^{-1}. \tag{26}$$

This finally proves Eq. (23). If at least one of the eigenvalues of $\tilde{\boldsymbol{U}}(\tau)$ has a modulus greater than or equal to 1, then Eq. (23) can be satisfied only for a particular choice of initial condition $\underline{\tilde{X}}(0)$ belonging to a subspace of dimension smaller than 3.

This condition on the eigenvalues of $\tilde{\boldsymbol{U}}(\tau)$ does not seem to have been appreciated before. It is quite important as we find regular instances of time allocations for which it is violated and the system energy diverges with time [white regions of Fig. 3(a)].

The present method allows us to determine analytically the equilibrium solutions and to classify their stability with certainty. Reference [6] presented the possibility of obtaining an analytical expression for the limit cycle going through the geometric series [Eq. (26)], but we find our procedure using the evolution matrices more transparent and straightforward.

Even though here we chose a time dependence of ω for which the analytical solution is available, the limit-cycle method can be useful also in other cases. If, in a different case, the analytical solution is not available, then it is possible to numerically integrate Eq. (16) for one cycle and apply the same procedure to calculate the equilibrium points from the matrix $\boldsymbol{U}(\tau)$.

In our case the analytical solution to the equation of motion exists and we compute the analytical expression of the limit-cycle solution $\underline{\tilde{X}}^0$, employing symbolic computation techniques. However, since these expressions are very long and not particularly insightful, they will not be presented here.

III. THERMODYNAMICS

A. Heat and work

The energy exchange of the system with the exterior through the different mechanisms is always given by the variation of the expectation value, $\langle \hat{H} \rangle$, of the Hamiltonian operator. However, in the context of the quantum heat engine it is necessary to analyze this energy exchange contribution more in detail. We introduce the number operator, denoted by $\hat{N}$, which satisfies the following relation involving ω and $\hat{H}$:

$$\hat{H} = \hbar\omega\left(\hat{N} + \frac{1}{2}\right). \tag{27}$$

The total energy exchange rate $d\langle \hat{H} \rangle/dt$ can always be expressed in terms of $N = \langle \hat{N} \rangle$ and ω:

$$\frac{d}{dt}\langle \hat{H} \rangle = \underbrace{\hbar\frac{d\,\omega}{dt}\left(\langle \hat{N} \rangle + \frac{1}{2}\right)}_{\propto\,\dot{\omega}} + \underbrace{\hbar\omega\frac{d}{dt}\langle \hat{N} \rangle}_{\propto\,\dot{N}}. \tag{28}$$

During the isochoric processes the frequency ω is constant and the first term of the right-hand side of Eq. (28) is zero: All the energy variation can be interpreted as heat exchanged with one of the thermal reservoirs.

It can be shown that during the adiabatic processes the two terms on the right-hand side of Eq. (28) correspond,

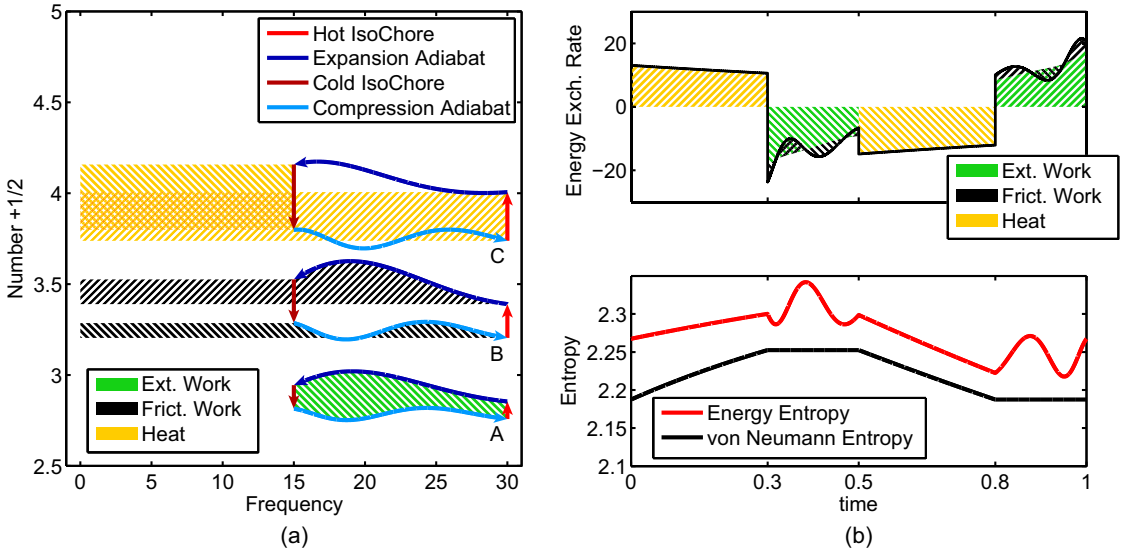

FIG. 1. Left panel: Three example cycles are used to illustrate the three contributions to the energy exchange rate. Positive contributions, i.e., entering the system, are patterned with lines with positive slope and negative contributions are patterned with lines with negative slope. Right top panel: The contributions to the energy exchange rate are plotted as functions of time. The total exchange rate is indicated by the black line. Right bottom panel: Energy entropy and von Neumann entropy are plotted as functions of time. The von Neumann entropy is always smaller than the energy entropy and the difference decreases during the dissipative processes.

respectively, to the first two matrix entries of Eq. (17):

$$+\omega(t)\mu H = \hbar\frac{d\,\omega}{dt}\left(N+\frac{1}{2}\right) \quad \text{and}$$
$$-\omega(t)\mu L = \hbar\omega\frac{d}{dt}N. \tag{29}$$

Following other authors [4,5], we distinguish between these two different contributions to the total power being exchanged with the system during the adiabatic processes. The first contribution is the *external work* while the second contribution is often called *frictional work*. As is pointed out in Ref. [5], this latter contribution to the total power is analogous to friction in the sense that it reduces the power, is zero when the motion is infinitely slow, and increases with speed.

The energy exchange mechanisms can be interpreted geometrically by plotting the cycle trajectory as a function of ω and $(N+\frac{1}{2})$. Three different limit cycles are shown in Fig. 1(a) and labeled by the letters A, B, and C. We decided to use three separate examples to illustrate the geometrical interpretation of the different energy exchange contributions, since using a single example would have made the figure more difficult to understand. For each case the cycle is subdivided into its four branches which are plotted in different colors. The shaded areas correspond to different energy exchange contributions.

The heat exchanged during the isochoric process is highlighted in orange for cycle C. Positive contributions are patterned with lines with positive slope and negative contributions are patterned with lines with negative slope. The frictional contribution to the total work is highlighted in black for cycle B. The net external work is highlighted in green for cycle A. As can be seen from Eq. (28), the external work exchanged during each adiabat process is equal to the area between the corresponding curve segment and the frequency (ω) axis. However, the interval of the omega axis spanned during the expansion adiabat is equal to the interval spanned during the compression adiabat, and the external work has opposite sign for the two processes. For this reason the contributions to the net external work due to the region not enclosed by the cycle curve cancel each other and the corresponding area is not shaded in example A of Fig. 1(a). This argument cannot be applied to the heat exchange and the frictional work, since the intervals of the N axis differ: The contributions due to the region not enclosed by the cycle curve do not cancel perfectly (examples B and C).

For limit-cycle trajectories energy conservation implies that the net heat exchanged during a cycle is equal in value and opposite in sign to the net total work exchanged. The same color code is applied to the top panel of Fig. 1(b), where the different energy exchange rates are plotted as functions of the time t for one example limit cycle. The thick black line represents the total energy exchange rate at any given moment.

The two contributions to the energy exchange can also be computed from the density operator $\hat{\rho}$ by expanding it over the time-dependent basis of the eigenstates of the Hamiltonian operator $\hat{H}$. Once $\hat{\rho}$ has been written in this form, the diagonal elements, P_n, of the matrix expansion correspond to the probability of occupation of the energy levels. The diagonal elements of $\hat{H}$, denoted by ε_n, are the eigenenergies. The total energy is then expressed by the sum $H(t)=\sum_n P_n(t)\varepsilon_n(t)$, and the following expression can be used to separate the two different contributions to the total power $\mathcal{P}_{\rm tot}$:

$$\mathcal{P}_{\rm tot}(t) = \frac{d}{dt}\sum_n P_n(t)\varepsilon_n(t)$$
$$= \underbrace{\sum_n \dot{P}_n(t)\varepsilon_n(t)}_{\text{Frictional}} + \underbrace{\sum_n P_n(t)\dot{\varepsilon}_n(t)}_{\text{External}}. \tag{30}$$

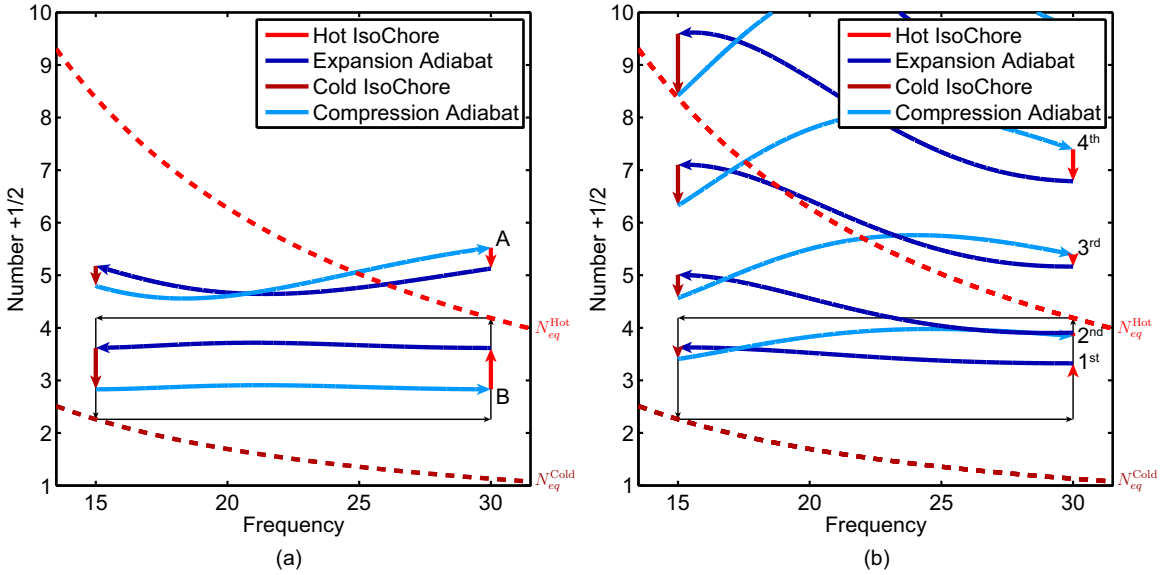

FIG. 2. Different example cycles are used to illustrate the different possible categories of solutions. The cycle trajectories are plotted as functions of ω and $(N+\frac{1}{2})$. Left panel: The trajectory labeled by B is a normal enginelike cycle which provides a positive net power. The thin black rectangle is the reversible (long-time limit) cycle, touching the hot and cold reservoirs at two corners. For the trajectory labeled by A the heat transfer during the hot isochoric process has the opposite sign (out of the system), resulting in negative power produced. These kinds of cycles are indicated in Figs. 3, 5, and 6 by the color gray. Right panel: A trajectory, starting at the lower right marked "1st" is winding its way upward. Thus the system is not able to converge to a limit cycle. These kinds of trajectories are indicated in Figs. 3, 5, and 6 by the color white.

According to the adiabatic theorem, the frictional contribution of the work converges to zero in the quasistatic limit, i.e., when the time allocated for the adiabatic process is very long.

B. Entropy

Many thermodynamic quantities are uniquely defined by the value of $\underline{X} = (H, L, C)$, and closed-form expressions can be derived. The more relevant definitions for the case of the quantum heat engine are the von Neumann entropy and the energy entropy.

The *von Neumann entropy* S_{vN} is defined as

$$S_{\mathrm{vN}}[\hat{\rho}] = -\mathrm{Tr}[\hat{\rho}\log(\hat{\rho})]. \tag{31}$$

The *energy entropy* is defined in term of the occupation probabilities P_n of the energy levels of the Hamiltonian $\hat{H}$ as

$$S_{\hat{H}} = -\sum_n P_n \log(P_n). \tag{32}$$

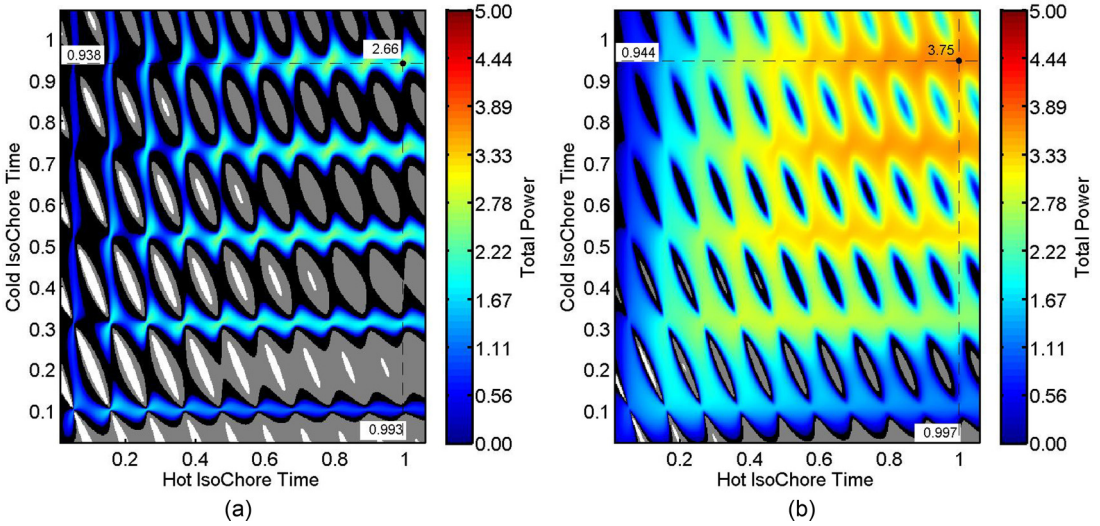

FIG. 3. The total power $\overline{\mathcal{P}}_{\mathrm{tot}}$ is plotted on the (τ_H, τ_C) plane. The power landscape exhibits a periodic structure with a period equal to π/ω_H in the τ_H direction and to π/ω_C in the τ_C direction. The left panel shows the case of short adiabat times, $\tau_{HC} = \tau_{CH} = 0.08$, where cycles which do not produce a positive total power occur more frequently than for intermediate adiabat times, $\tau_{HC} = \tau_{CH} = 0.227$, shown in the right panel. Maximum power is produced at the intersection of the dashed lines. The color scheme is explained in Se. IV A.

We calculate S_{vN} and $S_{\hat{H}}$ from the values of H, L and C, as explained in Ref. [5]. Different characteristics of the time dependence of these entropies can be theoretically predicted. The von Neumann entropy is a lower limit with respect to the entropy of any operator, including $\hat{H}$. During adiabatic processes the von Neumann entropy is expected to remain constant while the energy entropy may vary if the process is not in the quasistatic limit. For an isochoric process the density operator is expected to converge to the thermal equilibrium state which is diagonal in the energy basis. For this reason the difference between S_{vN} and $S_{\hat{H}}$ is expected to decrease during the dissipative dynamics. This phenomenon is an effect of the decoherence mechanism which is also linked with the decrease of the amplitude of the oscillation of L and C. Moreover, during the cooling isochore the von Neumann entropy should decrease. In the bottom panel of Fig. 1(b) the von Neumann entropy and the energy entropy are plotted as functions of time for a complete cycle of the engine. All the features described above may be observed in this graph.

IV. RESULTS

A. Optimization setup

The objective of the optimization problem that is most studied in the literature in the context of quantum heat engines is maximization of the average total power with respect to the choice of the four times allocated for the four different branches of the thermodynamic cycle. The total power $\overline{\mathcal{P}}_{\mathrm{tot}}$ is defined as the net energy exchanged during the adiabatic processes divided by the total duration of one cycle,

$$\overline{\mathcal{P}}_{\mathrm{tot}} = -\frac{\mathcal{W}_{\mathrm{tot}}}{\tau} = -\frac{1}{\tau}\int_{\mathrm{adiabats}} \frac{dH}{dt}\, dt. \tag{33}$$

The minus sign is introduced because we are interested in maximizing the power *extracted* from the system. In the results we will show in this section, such as Figs. 3, 5, and 6, the total power $\overline{\mathcal{P}}_{\mathrm{tot}}$ is indicated by the color according to the color map shown on the side of the figure. Further, the different solutions can be classified in categories depending on their behavior with respect to the objective function. Some special cases are illustrated in Figs. 2(a) and 2(b) by the cycle trajectories as functions of ω and $(N + \frac{1}{2})$.

(1) Normal enginelike trajectories: The *color* of the power landscape in Figs. 3, 5, and 6 indicates the value of total power produced, ranging from blue (low power) to red (high power). An example of such a cycle corresponds to the trajectory labeled B in Fig. 2(a).

(2) Trajectories for which the heat transfers during the isochoric processes have the correct sign (into the system on hot isochores and out of the system on cold isochores), but net total power has the opposite sign, are indicated in Figs. 3, 5, and 6 by the color black.

(3) Trajectories for which the heat transfer during at least one of the isochoric processes has the opposite sign are indicated in Figs. 3, 5, and 6 by the color gray. An example of such a cycle corresponds to the trajectory labeled A in Fig. 2(a).

(4) Trajectories for which the system is not able to converge to a limit cycle are indicated in Figs. 3, 5, and 6 by the color white. This behavior corresponds to the cases for which at least one of the eigenvalues of the matrix $\tilde{\boldsymbol{U}}(\tau)$ defined in Eq. (20) has norm greater than or equal to 1. An example of evolution over the time span of several cycles can be seen in Fig. 2(b). It may be noticed how N increases with time instead of exhibiting the expected cyclic behavior.

All the data points of the power landscapes shown in Figs. 3, 5, and 6 have been computed analytically using the techniques described in Sec. II and, in particular, the method illustrated in Sec. II G, which allows us to determine the closed-form expression of the limit cycle and classify its stability.

In order to be able to compare the different results of this section, the values of the engine parameters are kept constant for all the simulations that will be presented:

$$\omega_H = 30, \quad \omega_C = 15, \quad \beta_H = 0.008, \quad \beta_C = 0.03,$$
$$\Gamma_H = \Gamma_C = 0.7, \quad m = 1 \tag{34}$$

The adiabatic dynamics using a constant dimensionless parameter μ was used throughout. Further, we decided to adopt the convention that $\hbar$ and k_B are both equal to 1.

Figures 3(a) and 3(b) already present several peculiarities of the $\overline{\mathcal{P}}_{\mathrm{tot}}(\tau_H, \tau_C)$ power landscape. In both cases one observes a periodic structure superimposed on a slowly varying behavior. In the next section we will examine more in detail the occurrence of the periodic structure. Another interesting feature is that in both cases the power drops to zero when either τ_H or τ_C goes to zero. Since the power is equal to the total work divided by the total cycle time, it converges to zero also in the limit of long allocated times. This feature will be visible in the following figures which cover a larger area of the (τ_H, τ_C) plane. By comparing Fig. 3(a) with Fig. 3(b), we notice that the occurrence of normal enginelike cycles with positive power is more frequent for intermediate adiabat times than it is for short adiabat times. The white areas corresponding to conditions where it was not possible to achieve a closed limit cycle dominate at the very short times. These are strongly driven dissipative systems for which the isochore times are simply too short to obtain the necessary heat transfers, and an increasing amount of work is delivered to the system during the adiabats in an attempt to force the desired heat transfers. The excess energy builds up in the working fluid, making closure of the cycle impossible. Such divergence has not been reported previously for any quantum heat engine. The quantum mechanical origin of this periodic divergence is discussed in an upcoming article.

B. Frictionless cycles

We start the analysis of finding the optimal sets of times by considering a special class of solutions for which the system starts each of the four steps of the thermodynamic cycle in the completely noncoherent thermal state characterized by $\langle \hat{L} \rangle = \langle \hat{C} \rangle = 0$. This feature can be predicted by considering the analytical solution $\boldsymbol{U}^{\mathrm{adiabat}}$ of Eq. (17), as described in Ref. [7]. The requirement that $\langle \hat{L} \rangle = \langle \hat{C} \rangle = 0$ at the beginning of each step is related to the evolution matrices of the adiabatic processes. In particular, the matrix elements $U_{CH}^{\mathrm{adiabat}}$ and $U_{LH}^{\mathrm{adiabat}}$ connecting the operators $\hat{L}$ and $\hat{C}$ with the Hamiltonian $\hat{H}$ have to be zero at the final instant of each adiabatic process. This results in a condition on the duration of the adiabatic

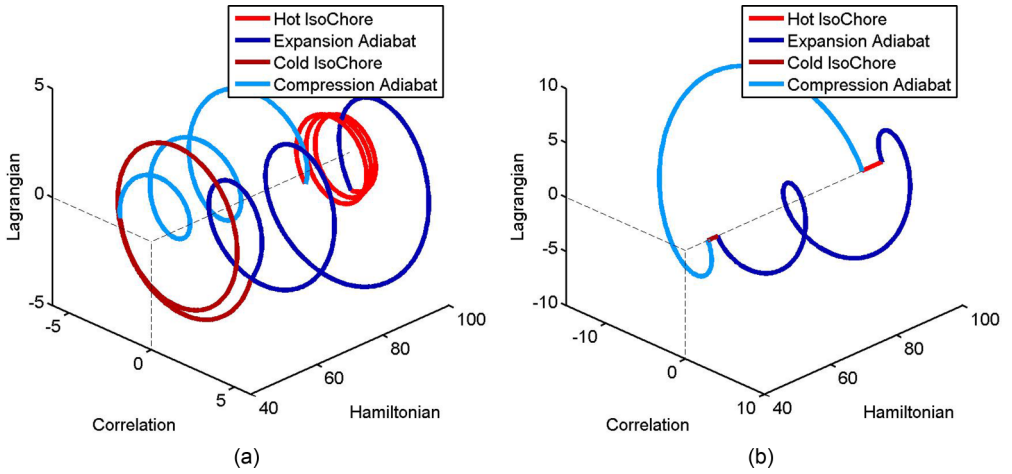

FIG. 4. Two limit-cycle trajectories plotted in the (H,L,C) space. The times allocated for the isochoric processes are $\tau_H = \tau_C = 0.3$. Left panel: Adiabat times $\tau_{HC} = \tau_{CH} = 0.4$. Right panel: A frictionless trajectory with adiabat times $\tau_{HC} = \tau_2$, $\tau_{CH} = \tau_1$. One notices that the values of L and C remain zero during both isochores for this frictionless trajectory.

processes which are then limited to a discrete infinite set τ_n:

$$\tau_n = \frac{1}{2}\left[\xi^2 + \left(\frac{2n\pi}{\gamma}\right)^2\right]^{1/2} \quad \text{with} \quad \xi = \frac{\omega_f - \omega_i}{\omega_f \omega_i} \quad \text{and} \quad \gamma = \frac{\ln(\omega_f/\omega_i)}{\xi}. \tag{35}$$

Note that the values of τ_n are invariant with respect to exchange of initial frequency ω_i and final frequency ω_f, leading to the same result for both adiabatic processes. In our examples, the hot and cold frequencies are respectively equal to 30 and 15, leading to the following values for the first solutions: $\tau_1 \approx 0.152$ and $\tau_2 \approx 0.303$.

Figure 4(b) shows one example of this class of solutions, plotted in the three-dimensional space (H,L,C), which can be compared to the general trajectory shown in Fig. 4(a). As expected, at the beginning of each step of the example of Fig. 4(b) the expectation values of $\hat{L}$ and $\hat{C}$ are zero and they remain zero during the whole duration of the isochoric processes. The values of the two adiabat times do not have to be equal; this example corresponds to the choice $\tau_{HC} = \tau_2$ and $\tau_{CH} = \tau_1$, (with $\tau_H = 0.3$ and $\tau_C = 1.13$).

The fact that the expectation values L and C remain zero for the whole duration of the isochoric processes implies that the solution will not exhibit a periodic dependence with respect to τ_H and τ_C. The total power $\overline{\mathcal{P}}_{\text{tot}}$ landscape on the (τ_H,τ_C) plane for a choice of adiabat times that satisfy this condition ($\tau_{HC} = \tau_2 \approx 0.303$, $\tau_{CH} = \tau_1 \approx 0.152$) is plotted in Fig. 5(b). As can be seen, the appearance of the power landscape with respect to the isochore times is smooth and slowly varying, and all limit cycles close (there are no white areas).

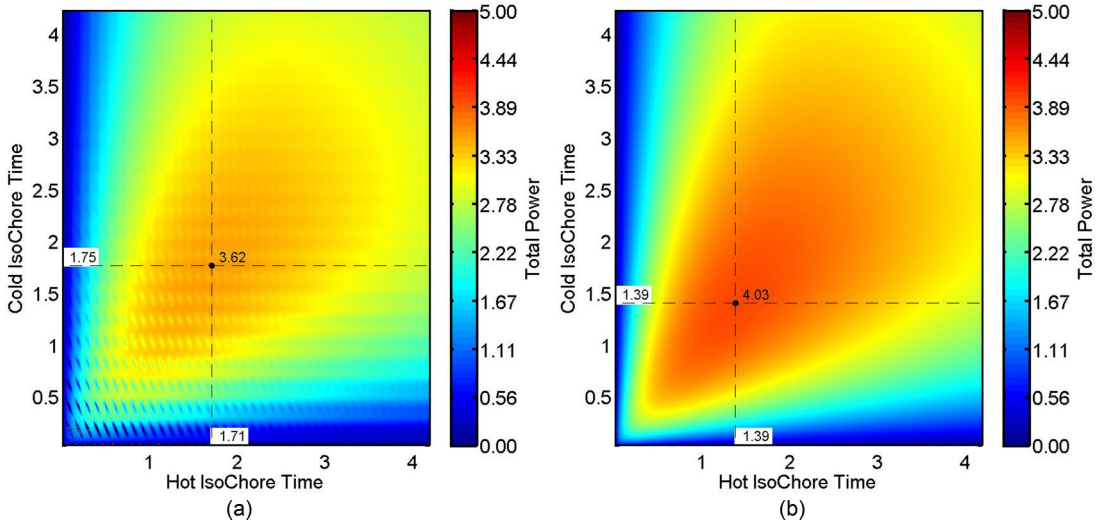

FIG. 5. The total power $\overline{\mathcal{P}}_{\text{tot}}$ is plotted on the (τ_H,τ_C) plane. Left panel: The power landscape corresponding to a general choice of adiabat times, $\tau_{HC} = \tau_{CH} = 0.4$, and therefore exhibiting the periodic structure. Right panel: The power landscape corresponding to adiabat times resulting in frictionless cycles, $\tau_{HC} = \tau_2$, $\tau_{CH} = \tau_1$. These do not exhibit the periodic structure. The optimal points are visible at the intersection between the black dashed lines. The color scheme is explained in Sec. IV A.

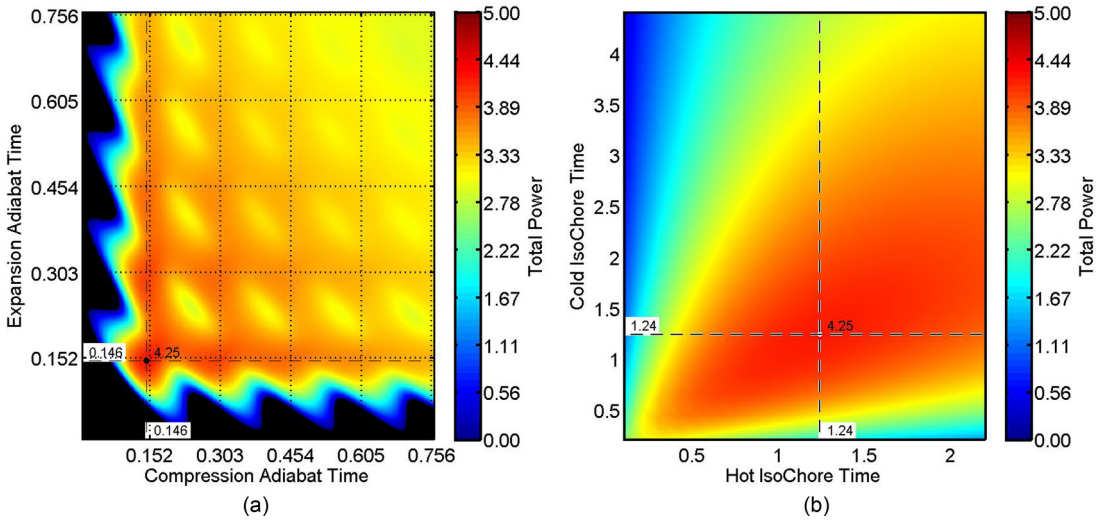

FIG. 6. Left panel: The total power $\overline{\mathcal{P}}_{\rm tot}$ is plotted on the (τ_{HC},τ_{CH}) plane of adiabat times for the isochore times $\tau_H = \tau_C = 1.24$. One notices the periodic structure determined by the set of times τ_n defined in Eq. (35) and drawn as the grid in dotted line. Right panel: The optimal values $\overline{\mathcal{P}}^{\rm opt}_{\rm tot}$ with respect to the adiabat times τ_{HC} and τ_{CH} plotted as a function of τ_H and τ_C. The optimal point of this plane is thus the global maximum. The color scheme is explained in Sec. IV A.

This can be compared with the result for a choice that does not satisfy this condition ($\tau_{HC} = \tau_{CH} = 0.4$). The same region of the (τ_H,τ_C) plane is plotted for this case in Fig. 5(a). The appearance of the landscape is characterized by a strong periodicity with respect to τ_H and τ_C superimposed on a slowly varying behavior already visible in the previous case. The evolution equations predict that the period of the oscillations in the τ_H and τ_C directions are, respectively, equal to π/ω_H and π/ω_C. The optimal total power point is visible in both figures at the intersection between the black dashed lines.

The total power $\overline{\mathcal{P}}_{\rm tot}$ exhibits a periodic structure also when plotted as function of the adiabat times τ_{HC} and τ_{CH}, as is seen from Fig. 6(a). In this case the periodic structure is determined by the set of times τ_n, defined in Eq. (35). It is also important to notice that there actually is a unique point of the grid with maximum power production and that it is located extremely close to the frictionless point $\tau_{HC} = \tau_{CH} = \tau_1$, but not exactly on it, at slightly shorter times. This result indicates that the maximum net power is achieved with a trajectory that is not perfectly frictionless, but the (slight) frictional loss is balanced by a faster rate of operation and thus larger power.

The last result of our optimization study is illustrated in Fig. 6(b). The total power $\overline{\mathcal{P}}_{\rm tot}$ is optimized with respect to the adiabat times τ_{HC} and τ_{CH} for different combinations of τ_H and τ_C:

$$\overline{\mathcal{P}}^{\rm opt}_{\rm tot}(\tau_H,\tau_C) = \max_{\tau_{HC},\tau_{CH}} [\overline{\mathcal{P}}_{\rm tot}(\tau_H,\tau_{HC},\tau_C,\tau_{CH})]. \qquad (36)$$

The optimized values of power $\overline{\mathcal{P}}^{\rm opt}_{\rm tot}$ are then plotted as a function of τ_H and τ_C. The optimal point on this plane, visible at the intersection between the black dashed lines, is thus the globally optimal point with respect to our optimization problem. Since in Fig. 6(a) we selected the same isochore times of the global maximum, the optimal point of this plane is also the global optimum. Note that in both cases the global optimum is an interior point, i.e., there is an optimal total cycle time τ. At short times friction becomes too large and there is not enough time to recover it, while at long times the turnover of the engine is too slow.

V. CONCLUSION

We investigated the behavior of a quantum Otto cycle whose working medium is composed of an ensemble of harmonic oscillators. We introduced an analogy between our system state vector and homogeneous coordinates which allowed us to employ exclusively analytical methods for the calculation of each limit-cycle solution, as well as for the classification of its stability.

As is traditional in the field of finite-time thermodynamics, we adopted an optimization point of view: We addressed the problem of extracting the maximum amount of power output from the quantum engine by selecting the times allocated for each of the four branches of one cycle. An interior global maximum power point is located for a given total cycle time τ. Particularly for short time cycles, it is necessary to be careful in the selection of meaningful cycles in relation to the goal of power optimization. For some cycles the frictional contribution dominates the behavior, preventing the system from reaching a limit cycle or leading to cycles characterized by a negative power output.

We draw a link between the special frictionless trajectories, which can be obtained by careful selection of the times allocated for the adiabat processes, and the appearance of the power landscape when plotted as a function of the allocated times. These special trajectories are a useful starting point to solve our optimization problem since the global optimum lies close to one of these.

ACKNOWLEDGMENTS

The authors thank Ronnie Kosloff for helpful discussions, in particular pointing out the importance of the diverging trajectories.

[1] H. P. Breuer and F. Petruccione, *The Theory of Open Quantum Systems*, Vol. 116 (Oxford University Press, Oxford, 2002), pp. 91–96.
[2] G. Lindblad, Commun. Math. Phys. **48**, 119 (1976).
[3] E. Geva and R. Kosloff, J. Chem. Phys. **97**, 4398 (1992).
[4] T. Feldmann and R. Kosloff, Phys. Rev. E **73**, 025107(R) (2006).
[5] Y. Rezek and R. Kosloff, New J. Phys. **8**, 83 (2006).
[6] Y. Rezek, Master's thesis, Hebrew University, Jerusalem, Israel, 2004.
[7] Y. Rezek, P. Salamon, K. H. Hoffmann, and R. Kosloff, Europhys. Lett. **85**, 30008 (2009).
[8] R. Kosloff and T. Feldmann, Phys. Rev. E **82**, 011134 (2010).
[9] F. L. Curzon and B. Ahlborn, Am. J. Phys. **43**, 22 (1975).
[10] P. Salamon, A. Nitzan, B. Andresen, and R. S. Berry, Phys. Rev. A **21**, 2115 (1980).
[11] B. Andresen, P. Salamon, and R. S. Berry, J. Chem. Phys. **66**, 1571 (1977).
[12] T. Feldmann and R. Kosloff, Phys. Rev. E **85**, 051114 (2012).
[13] Y. Rezek, Entropy **12**, 1885 (2010).